Chaos

Wave-packet spreading in disordered soft architected structures

Cite as: Chaos **32**, 053116 (2022); https://doi.org/10.1063/5.0089055
Submitted: 22 February 2022 • Accepted: 20 April 2022 • Published Online: 09 May 2022

A. Ngapasare, G. Theocharis, O. Richoux, et al.

AIP Publishing

Wave-packet spreading in disordered soft architected structures

Cite as: Chaos **32**, 053116 (2022); doi: 10.1063/5.0089055
Submitted: 22 February 2022 · Accepted: 20 April 2022 ·
Published Online: 9 May 2022

A. Ngapasare,[1,2,a)] G. Theocharis,[2] O. Richoux,[2] Ch. Skokos,[1] and V. Achilleos[2]

AFFILIATIONS

[1]Nonlinear Dynamics and Chaos Group, Department of Mathematics and Applied Mathematics, University of Cape Town, Rondebosch 7701, South Africa
[2]Laboratoire d'Acoustique de l'Université du Mans (LAUM), UMR 6613, Institut d'Acoustique—Graduate School (IA-GS), CNRS, Le Mans Université, Le Mans, France

[a)]**Author to whom correspondence should be addressed:** angapasare@gmail.com

ABSTRACT

We study the dynamical and chaotic behavior of a disordered one-dimensional elastic mechanical lattice, which supports translational and rotational waves. The model used in this work is motivated by the recent experimental results of Deng *et al.* [Nat. Commun. **9**, 1 (2018)]. This lattice is characterized by strong geometrical nonlinearities and the coupling of two degrees-of-freedom (DoFs) per site. Although the linear limit of the structure consists of a linear Fermi–Pasta–Ulam–Tsingou lattice and a linear Klein–Gordon (KG) lattice whose DoFs are uncoupled, by using single site initial excitations on the rotational DoF, we evoke the nonlinear coupling between the system's translational and rotational DoFs. Our results reveal that such coupling induces rich wave-packet spreading behavior in the presence of strong disorder. In the weakly nonlinear regime, we observe energy spreading only due to the coupling of the two DoFs (per site), which is in contrast to what is known for KG lattices with a single DoF per lattice site, where the spreading occurs due to chaoticity. Additionally, for strong nonlinearities, we show that initially localized wave-packets attain near ballistic behavior in contrast to other known models. We also reveal persistent chaos during energy spreading, although its strength decreases in time as quantified by the evolution of the system's finite-time maximum Lyapunov exponent. Our results show that flexible, disordered, and strongly nonlinear lattices are a viable platform to study energy transport in combination with multiple DoFs (per site), also present an alternative way to control energy spreading in heterogeneous media.

In recent years, substantial advances have been made in the field of architected elastic devices following the large interest in studies of metamaterials. These studies on architected materials have unearthed some exceptional structural, conformational, thermal, topological, and vibrational properties in both the linear and nonlinear regimes. However, in spite of all these advances, the study of wave propagation in the presence of disorder for such architected materials with several degrees of freedom is still missing. Using an experimentally verified model for a soft architected material made from LEGO® bricks, we investigate wave-packet spreading and the chaotic behavior of localized initial excitations. We characterize energy spreading using the exponent of the second moment of the energy distribution, and we find two distinct behaviors between the weakly and highly nonlinear regimes. In fact, we observe almost ballistic energy spreading when the nonlinearity is sufficiently strong for single site initial angular deflections. The chaoticity of the system, as measured by estimating the maximum Lyapunov exponent, is in-between the already known behaviors of the weak and strong chaos regimes of the disordered nonlinear Klein–Gordon and nonlinear Schrödinger lattices.

I. INTRODUCTION

Wave propagation in heterogeneous complex media has been a subject of intensive research interest in recent years. Among various systems, a large part of the conducted studies has been concentrated in families of one-dimensional (1D) continuous and discrete models[1–4] by focusing mainly on the localization properties of both the normal modes of finite systems, i.e., Anderson localization (AL),[5] as well as wave propagation in infinite media. The successful extension of AL to many other systems after it was initially formulated for electronic systems has opened many research

frontiers and applications.[6–10] Experimental results on AL (see, e.g., Refs. 7–11) have stimulated further interest in AL for both quantum and classical systems.

Regarding linear disordered 1D lattices, among different systems, special attention has been given to the tight binding electron model,[12] the linear Klein–Gordon (KG) lattice,[13] and the harmonic lattice.[1,14–16] These models are not only relevant to various physical systems but also represent the linear limits of seminal nonlinear lattices, such as the discrete nonlinear Schrödinger equation (DNLS), the quartic KG, and the Fermi–Pasta–Ulam–Tsingou (FPUT) lattices.[3,17–19] Within the context of phononic and photonic lattices, these fundamental models have been adopted to describe a variety of physical systems, and more recently, they have been used as a testbed for novel wave phenomena.[20,21]

A common route to study the wave properties of disordered lattices is through monitoring the time evolution of initially compact wave-packets. For tight binding and linear KG models, the dynamics after the excitation of such an initial condition is characterized by a transient initial phase of spreading, followed by a phase of total confinement to the system's localization length. The width of the wave-packet is of the order of the maximum localization length.[22] On the other hand, for the harmonic lattice, along with the localized portion of the energy, there is always a propagating part due to the existence of extended modes at low frequencies. A quantitative description of wave propagation in disordered 1D systems of one degree of freedom (DoF) per lattice site was formulated in Refs. 14, 16, and 23 where wave-packet spreading was quantified using both analytical and numerical methods. Moreover, many variations of these 1D lattices have been studied extensively in several works, including dynamical regimes ranging from the homogeneous linear to the disordered nonlinear.[11,24–32]

As a natural extension to the above studies, an investigation into the corresponding behavior in disordered lattices with more than one DoF per site seems plausible. Not many studies along such lines have been reported in the literature. The majority of existing works has taken the approach of making generalizations of the tight binding model by assuming a linear coupling between two (or more) 1D chains.[33,34] Such coupling results in changes to the dispersion relation, thereby changing the energy transport properties. Our recent work with a linear disordered phononic lattice[35] is indeed an attempt to fill this gap. The wave dynamics of disordered harmonic chains with two DoFs per site appear to be quite interesting, deserving further investigations. Such systems have been useful in modeling macroscopic mechanical devices, including granular chains, highly deformable elastic assemblies, and origami lattices.[36–41] This allows for easy tunability of the system's dispersion due to the geometrical characteristics and material properties and makes these systems attractive for several applications.

Here, we focus on highly deformable architected lattices, characterized by a nonlinear response, which enabled the design of new classes of tunable and responsive elastic materials. Several such soft structures have already been reported, including bioinspired soft robots,[42,43] self-regulating microfluidics,[44] reusable energy absorbing systems,[45,46] materials with programmable response,[47] and information processing via physical soft bodies.[48] Furthermore, soft architected materials present opportunities to control the propagation of elastic waves since their dispersion properties can be altered by applying a large, nonlinear pre-deformation[49–51] or changing the geometry.[40] To date, most of the investigations have predominantly focused on linear stress waves or soliton solutions of such systems due to the capability of the soft structures to support large-amplitude nonlinear waves. Here, taking a step forward, we study a particular lattice that supports both translational and rotational waves.[40] Our main goal is to understand how nonlinear lattice waves propagate in the presence of strong disorder when the DoFs are coupled, as well as the system's chaoticity.

The rest of this paper is arranged as follows: In Sec. II, we describe the Hamiltonian model of the lattice structure and also formulate the system's equations of motion. The dispersion relation of the system, in addition to its dynamics in the linear limit, is also discussed. In Sec. III, we investigate the nonlinear effects on wave propagation under strong disorder, as well as study the system's chaoticity, and finally, in Sec. IV, we summarize our findings and present our conclusions.

II. THE HAMILTONIAN MODEL AND ITS EQUATIONS OF MOTION

The 1D elastic mechanical lattice studied in this work is assembled from an array of aligned LEGO® crosses connected by flexible links[52] as depicted in Fig. 1. This system constitutes a highly deformable elastic lattice supporting both translational and rotational waves (2 DoFs per site). In Ref. 40, the authors describe the general equations of motion for a structure that takes into consideration some of the possible geometrical variations of the lattice. However, for the purposes of this work, we limit ourselves to an aligned, symmetrical structure. The crosses are joined to their neighbors by some flexible hinges, which are modeled using a combination of three linear springs. The stretching is modeled by a spring with stiffness k_l and the shearing is described by a spring k_s, while the bending is modeled by a torsional spring k_θ [see Fig. 1(b)].

By making use of the spatial periodicity a, we recast the horizontal deflections u_n at the nth lattice site to $U_n = u_n/a$ and change time units to dimensionless time, $T = t\sqrt{k_l/\overline{m}}$, and the springs are normalized as $K^{(\theta)} = 4k_\theta/k_l a^2$ and $K^{(s)} = k_s/k_l$. The mass of each unit of the cross m_n is normalized such that $M_n = m_n/\overline{m}$, where $\overline{m}$ is the average mass of the crosses. Similarly, the rotational moment of inertia of each cross J_n is normalized to give the dimensionless rotational moment of inertia Γ_n. Herein, $J_n = \frac{1}{6} m_n^{\dagger} (d^2 + b^2)$ denotes the rotational moment of inertia at the nth lattice site where the mass, length, and width of either the horizontal or vertical strip component of the cross is, respectively, denoted by $m_n^{\dagger}$, d, and b.[53] This implies that in the case of the homogeneous chain, $M = M_n = m_n/\overline{m} = 1$ and $\Gamma = \Gamma_n = J_n/(\overline{m}a^2) \approx 0.0759$. For the rest of this work, we assume the parameters of the experimental setup of Ref. 40 where each cross has mass $m = 4.52\,\mathrm{g}$ ($\overline{m} = m$), $a = 42\,\mathrm{mm}$, and $J = 605\,\mathrm{g\,mm^2}$. Also, the spring constants are $k_l = 71.69\,\mathrm{N\,mm^{-1}}$, $k_s = 1.325\,\mathrm{N\,mm^{-1}}$, and $k_\theta = 4.85\,\mathrm{N\,mm}$. It is worth noting that for the real LEGO® experiment in Ref. 40, each rigid unit is supported on pins such that friction and damping are negligible (detailed information is given in the supplementary material of Ref. 40).

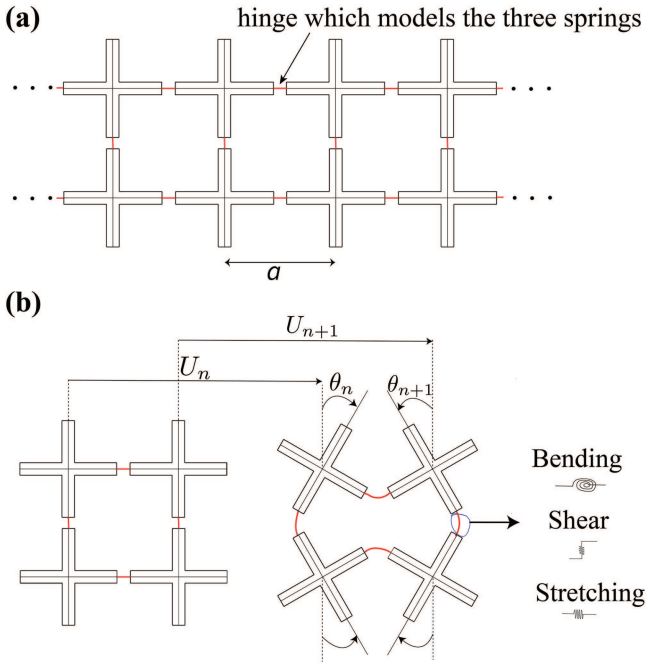

FIG. 1. (a) An architected, highly deformable, and elastic mechanical structure that supports translational and rotational waves. (b) Schematic of the cross pairs [by symmetry, the dynamics can be described by either the top row or the bottom row of (a)] showing the translational and angular deflections. The connectors (marked in red) model a combination of bending k_θ, shear k_s, and stretching springs k_l.

The Hamiltonian H of the top or bottom layer of the system is thus given as (see Ref. 40 for details)

$$H = \sum_{n=1}^{N} \left\{ \frac{M_n \dot{U}_n^2}{2} + \frac{\Gamma_n \dot{\theta}_n^2}{2} + \frac{1}{2}\Delta_{LH}^{n^2} + \frac{K^{(s)}}{2}\Delta_{SH}^{n^2} + \frac{K^{(\theta)}}{8}\left(\delta_{\theta H}^{n^2} + \frac{1}{2}\delta_{\theta V}^{n^2}\right)\right\}, \tag{1}$$

where the dimensionless deflections are given by $\Delta_{LH}^n = U_{n+1} - U_n + \frac{1}{2}(2 - \cos\theta_n - \cos\theta_{n+1})$, $\Delta_{SH}^n = \frac{1}{2}(\sin\theta_{n+1} - \sin\theta_n)$, $\delta_{\theta H}^n = \theta_{n+1} + \theta_n$, and $\delta_{\theta V}^n = 2\theta_n$. In Eq. (1), $\dot{[]}$ denotes the derivative with respect to time.

We derive the equations of motion from the Hamiltonian equation (1), which yields

$$M_n\ddot{U}_n = \left[U_{n+1} - U_n + \frac{1}{2}\{2 - \cos(\theta_n) - \cos(\theta_{n+1})\}\right] - \left[U_n - U_{n-1} + \frac{1}{2}\{2 - \cos(\theta_n) - \cos(\theta_{n-1})\}\right], \tag{2}$$

$$\begin{aligned}\Gamma_n\ddot{\theta}_n = {} & \frac{1}{4}K^{(s)}\cos(\theta_n)\,[\sin(\theta_{n+1}) - \sin(\theta_n)] \\ & + \frac{1}{4}K^{(s)}\cos(\theta_n)\,[\sin(\theta_{n-1}) - \sin(\theta_n)] \\ & + \frac{1}{4}\sin(\theta_n)\,[2(U_n - U_{n+1}) + \cos(\theta_n) + \cos(\theta_{n+1}) - 2] \\ & + \frac{1}{4}\sin(\theta_n)\,[2(U_{n-1} - U_n) + \cos(\theta_n) + \cos(\theta_{n-1}) - 2] \\ & - \frac{1}{4}K^{(\theta)}(\theta_{n+1} + 4\theta_n + \theta_{n-1}).\end{aligned} \tag{3}$$

A. Homogeneous linear system

First, let us consider the homogeneous system and linearize the nonlinear terms (trigonometric terms) in Eqs. (2) and (3) by assuming small angles, θ_{n+p} with $p = \{-1, 0, 1\}$, and taking a power series expansion of the appropriate cosine and sine terms to give the first two lowest order terms as

$$\sin\theta_{n+p} \approx \theta_{n+p} - \frac{1}{6}\theta_{n+p}^3 + \cdots, \tag{4}$$

$$\cos\theta_{n+p} \approx 1 - \frac{1}{2}\theta_{n+p}^2 + \cdots. \tag{5}$$

The linear parts of Eqs. (4) and (5) are plugged appropriately into Eqs. (2) and (3) to give the linear equations of motion as

$$M_n\ddot{U}_n = U_{n+1} - 2U_n + U_{n-1} \tag{6}$$

and

$$\Gamma_n\ddot{\theta}_n = \tilde{K}(\theta_{n+1} - 2\theta_n + \theta_{n-1}) - 6K^{(\theta)}\theta_n, \tag{7}$$

where $\tilde{K} = K^{(s)} - K^{(\theta)}$. For the homogeneous case, $M_n = M = 1$ and $\Gamma_n = \Gamma$ as already defined. A quick glance at Eqs. (6) and (7) reveals that the two sets of DoFs are decoupled in the linear regime. Equation (6) belongs to the linear FPUT class of equations, and Eq. (7) is a linear KG-type equation.

We now consider solutions of the form

$$\mathbf{X}_n = \begin{pmatrix} U_n(t) \\ \theta_n(t) \end{pmatrix} = \mathbf{X}\, e^{i\omega t - iqn}, \tag{8}$$

where $\mathbf{X} = [U_0, \Theta_0]$ is the amplitude vector, ω is the cyclic frequency, and q is the wave number. Inserting Eq. (8) into Eqs. (6) and (7), we obtain the following eigenvalue problem for the allowed frequencies $\mathbf{DX} = \Omega^2\mathbf{X}$, where the resultant dynamical matrix is

$$\mathbf{D} = \begin{pmatrix} 2 - 2\cos q & 0 \\ 0 & \frac{1}{2\Gamma}\left[(K^{(s)} + 2K^{(\theta)}) - (K^{(s)} - K^{(\theta)})\cos q\right] \end{pmatrix}.$$

The corresponding dispersion branch for the transverse DoFs is

$$\omega^{(U)} = \sqrt{2 - 2\cos q}, \tag{9}$$

while for the rotational DoFs,

$$\omega^{(\theta)} = \frac{1}{\sqrt{4\Gamma}}\sqrt{2\left(K^{(s)} + 2K^{(\theta)}\right) - 2(K^{(s)} - K^{(\theta)})\cos q}. \tag{10}$$

The dispersion relation for the two different DoFs, as given by Eqs. (9) and (10), is plotted in Fig. 2. An important feature for the

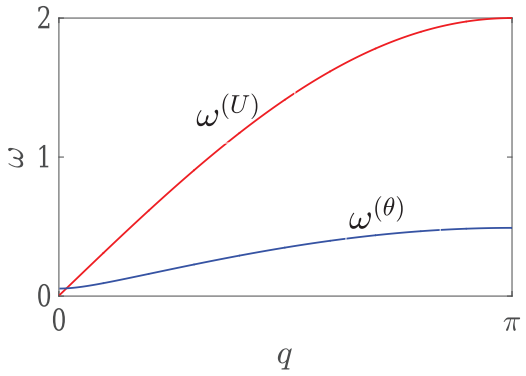

FIG. 2. The two dispersion branches of the system for translational ($\omega^{(U)}$—red curve) and rotational ($\omega^{(\theta)}$—blue curve) DoFs [see, respectively, Eqs. (9) and (10)].

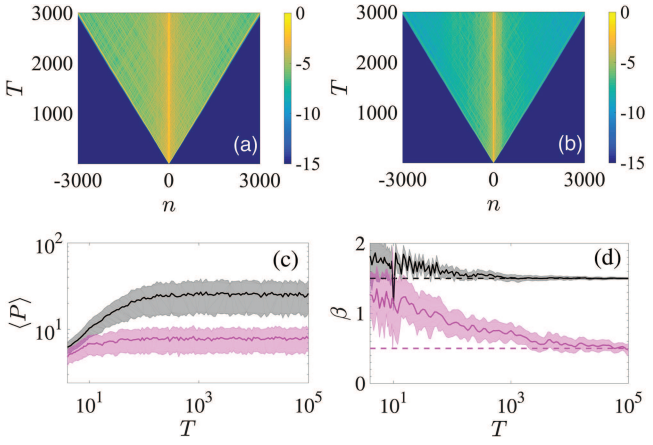

FIG. 3. Spatiotemporal evolution of the energy distribution for a representative realization with (a) velocity and (b) displacement single site initial excitation in the linear system. The colorbars in (a) and (b) are in log-scale. (c) Time evolution of the average participation number $\langle P\rangle$ and (d) estimation of the exponent β, related to the time evolution of the average second moment through $\langle m_2\rangle \propto T^{\beta}$. For velocity (black curves) and displacement (magenta curves) initial excitations, the mean values $\langle\cdot\rangle$ are calculated from 100 disorder realizations, and the shaded areas represent the statistical error (one standard deviation). The dashed lines in (d) indicate $\beta = 1.5$ (top) and $\beta = 0.5$ (bottom), and the system energy for all realizations is $H = 10^{-4}$.

system is that the rotational mode branch (blue curve in Fig. 2) starts at a finite frequency. This means that linear rotational waves are not supported for $\omega < \frac{1}{\sqrt{4\Gamma}}\sqrt{6K^{(\theta)}}$ since this frequency domain corresponds to a bandgap. In fact, the linear dispersion relation of the rotations can be directly mapped onto the one for the linear KG lattice. On the other hand, the transverse displacements follow a typical linear mass–spring dispersion relation.

B. Disordered linear system

In order to consider a disordered version of the system, we first note that the disordered linear KG system exhibits AL (see Ref. 16 for the corresponding behavior of the linear FPUT). Additionally, even though there are a number of ways to introduce disorder in the system, we model the crosses of the architected lattice assuming disorder in the masses M_n, which in turn implies disorder in the rotational moments of inertia Γ_n. In practice, disorder in the system can also be achieved by changing the material used to manufacture the LEGO® bricks at each site without changing their geometrical dimensions.[52,53] In dimensionless units, the masses are normalized to unity for a homogeneous chain; hence, we take this into consideration when choosing the disorder distribution and take M_n from a uniform probability distribution $f(M_n)$ where

$$f(M_n) = \begin{cases} W^{-1}, & -W/2 < M_n - 1 < W/2, \\ 0 & \text{otherwise.} \end{cases}$$

W denotes the distribution width, and for this study, we choose $W = 1.8$; hence, $0.1 \le M_n \le 1.9$.

To study the dynamical behavior of the system, the equations of motion are integrated using the **ABA864** symplectic integrator,[54] which has been proved to be very efficient for the accurate integration of large Hamiltonian lattice models.[55,56] This integration scheme allows for energy conservation of the total energy H and keeps the relative energy error $\Delta H(T) = \left|\frac{H(T) - H(0)}{H(0)}\right| < 10^{-5}$ when the integration time step is set to be $\tau = 0.1$. In all our numerical simulations, we employ fixed boundary conditions; i.e., $U_0 = U_{N+1} = 0$, $\theta_0 = \theta_{N+1} = 0$, $\dot{U}_0 = \dot{U}_{N+1} = 0$, and $\dot{\theta}_0 = \dot{\theta}_{N+1} = 0$. Furthermore, the considered lattice size is large enough so that the energy does not reach the lattice boundaries. A typical numerical integration of the nonlinear system for $T = 10^5$ requires a lattice size of at least 2×10^5 sites.

1. Translational degrees of freedom

We start our analysis by first exploring the two possible single site initial excitations of velocity and displacement for the translation DoFs; i.e.,

$$\dot{U}_{N/2}(0) = \sqrt{2H/M_{N/2}} \quad \text{or} \quad U_{N/2}(0) = \nu \tag{11}$$

independently. In Eq. (11), the scalar ν is real, and its value is altered to match the desired system energy. We fix the total system energy at $H = H_0$ and integrate the system up to $T = 10^5$ time units and observe how the initially localized wave-packet evolves in time. A typical scenario of the dynamics is shown in Figs. 3(a) and 3(b) for $H_0 = 10^{-4}$. For single site velocity initial excitations, the energy distribution displays two main parts: a central localized part and an expanding peripheral part, which is spreading beyond the excitation point [see Fig. 3(a)]. Similar spreading characteristics are observed in the dynamics for displacement initial excitations as depicted in Fig. 3(b).

For a more quantitative description, we follow the time evolution of the participation number P and the second moment m_2 of the energy distribution to characterize the localization and spreading properties of the wave-packet. The former quantity P is used to quantify the number of highly excited sites in a lattice[21] and is

computed as

$$P = 1/\sum h_n^2, \tag{12}$$

where $h_n = H_n/H$ is the normalization of the site energy H_n. In the case of equipartition, for a lattice of size N, $P = N$, while the other extreme gives $P = 1$, for a wave-packet in which only a single site is highly excited. The second moment m_2[16] of the energy distribution given by

$$m_2 = \sum_n (n - \overline{n})^2 H_n/H \tag{13}$$

is a measure of the wave-packet's extent where $\overline{n} = \sum_n nH_n/H$ is the mean position of the energy distribution.

The time evolution of $\langle P\rangle$ indicates that a maximum value is reached and remains constant for both velocity and displacement excitations as illustrated in Fig. 3(c) by the black and magenta curves, respectively. In this work, $\langle\cdot\rangle$ denotes averages over 100 disorder realizations. One of the differences between the two cases is that velocity initial excitations yield slightly higher values of $\langle P\rangle$ when compared to the $\langle P\rangle$ reached for displacement initial excitations. This is due to the fact that more low frequency propagating modes are excited for the case of velocity initial excitation than with displacement initial excitation.[16] The time evolution of $\langle m_2\rangle$ for the two excitations is also different for the same reason.

Regarding the second moment m_2, the usual practice is to assume that $\langle m_2\rangle \propto T^\beta$. Then, the parameter β is numerically estimated by the time local derivative

$$\beta = \frac{d\log_{10}\langle m_2(T)\rangle}{d\log_{10} T}. \tag{14}$$

The exponent β is used to quantify the asymptotic behavior of $\langle m_2\rangle$ for sufficiently large times. It is calculated by first smoothing the $m_2(T)$ values of each disorder realization through a locally weighted difference algorithm[57,58] and then averaged over all realizations. The computed β for the two cases saturates to $\beta = 1.5$ and $\beta = 0.5$ for, respectively, velocity and displacement single site excitations as shown in Fig. 3(d). This is an expected result because we have already shown the system to be practically a linear disordered FPUT lattice since the translational DoFs do not couple to the rotational DoFs. Here, we note that, according to the full system of equations [Eqs. (2)–(3)], single site translational excitations as given by Eq. (11) will never couple the two DoFs. This is a particularity of the structural geometry under consideration. Thus, whatever the initial excitation energy, single site initial translations will always lead to the linear behavior summarized in Fig. 3. For this reason, we shall not consider such initial conditions in Sec. III.

2. Rotational degrees of freedom

We now turn our attention to the dynamics of single site rotational excitations (angular deflection or the angular deflection time derivative). These excitations are expected to follow the dynamics of a discrete linear KG lattice as already explained earlier in Sec. II A.

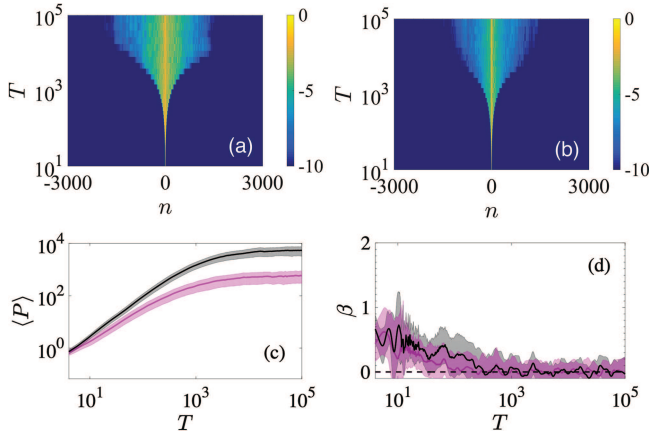

FIG. 4. Similar to Fig. 3 but for initial angular deflections (magenta curves) and angular deflection time derivatives (black curves). The vertical axes for (a) and (b) are given in $\log_{10}$. In (c), we show the time evolution of $\langle P\rangle$, and the dashed line in (d) indicates $\beta = 0$.

More specifically, we consider independently the initial excitations

$$\dot\theta_{N/2}(0) = \sqrt{2H/\Gamma_{N/2}} \quad \text{or} \quad \theta_{N/2}(0) = \mu, \tag{15}$$

where μ is real and is chosen to match the desired system energy $H = H_0$.

The energy distribution profiles for both angular deflection time derivative (black curves) and angular deflection (magenta curves) excitations [see Figs. 4(a) and 4(b)] show localized energy distributions for times $T \gtrsim 10^4$ after an initial phase of wave-packet spreading. The subtle differences between angular deflection time derivative and angular deflection initial excitations in panels (a)–(b) of Fig. 4 are mainly due to the differences in the initially excited modes of the system for each respective excitation. Thus, the dynamics of the rotations in the linear limit show complete localization in sharp contrast to the perpetual wave-packet spreading observed for the translational DoFs [Figs. 3(a) and 3(b)]. This is a consequence of the fact that the KG system [Eq. (7)] describing rotations is known to map to the DNLS and experiences localization of all modes.[59–61] To quantify the localization for the initial angular deflections (magenta curves) and angular deflection time derivatives (black curves), we plot the time evolution of $\langle P\rangle$, which reaches constant finite values after $T \gtrsim 4 \times 10^4$ [Fig. 4(c)]. A similar behavior is observed for $\langle m_2\rangle$ (not shown here) for $T \gtrsim 10^3$] in agreement to what is expected for a linear disordered KG chain. The final saturation of the $\langle m_2\rangle$ value is clearly depicted in the evolution of the exponent β from the relation $\langle m_2\rangle \propto T^\beta$, which eventually becomes $\beta = 0$ as clearly seen in Fig. 4(d), showing that indeed, the system is effectively a 1D linear disordered KG chain.

III. DISORDERED NONLINEAR SYSTEM

Having considered the behavior of the system in the linear limit, we further study the fully nonlinear system as described by Eqs. (2) and (3). Before proceeding further, we reiterate that single site initial translational velocity ($\dot U_{N/2}$) or displacement ($U_{N/2}$)

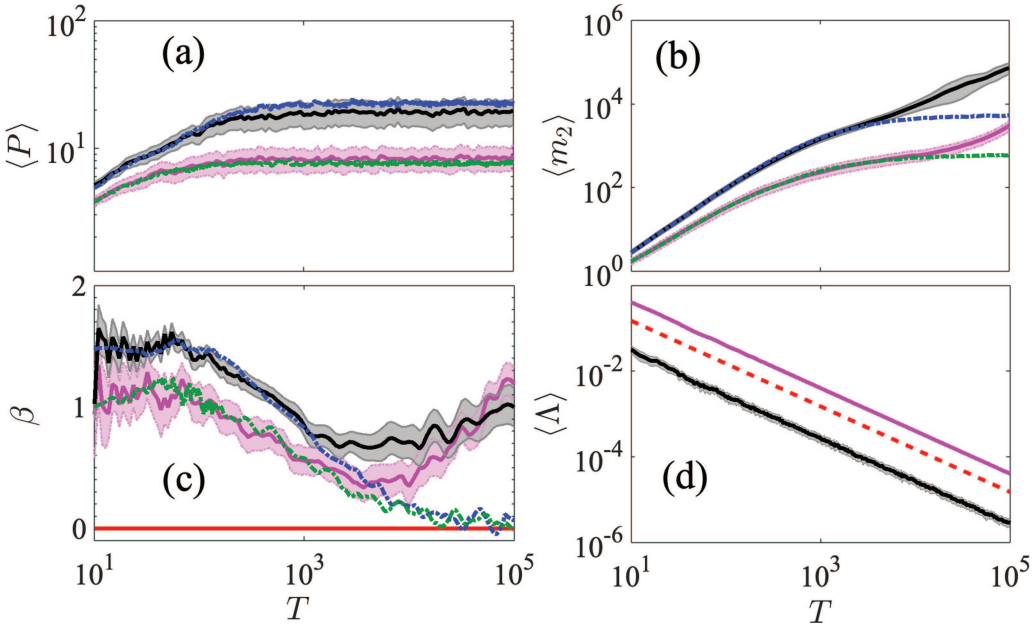

FIG. 5. Weakly nonlinear system: (a)–(d) Time evolution of $\langle P \rangle$ (12), $\langle m_2 \rangle$ (13), β (14), and $\langle \Lambda \rangle$ (16), respectively. The black (magenta) curves correspond to single site initial angular deflection time derivative (angular deflection) excitations. The average values $\langle \cdot \rangle$ are computed from 100 disorder realizations, and the lightly shaded areas represent the statistical error (one standard deviation). The dashed blue and green curves that are not always visible due to their overlapping with other curves, respectively, show results of the linearized system for the initial conditions given by Eq. (15). All results are for the weakly nonlinear regime with $H = 10^{-8}$. The horizontal line in (c) indicates $\beta = 0$.

excitations *do not induce a nonlinear response*. However, initial rotational excitations induce both a nonlinear response on rotations as well as nonlinear coupling between the two sets of DoFs. For the rest of this work, we focus exclusively on single site (in the center of the lattice) initial conditions of angular deflections as well as angular deflection time derivatives.

A. Weakly nonlinear regime

We start by implementing single site angular deflections and time derivatives of angular deflections as initial excitations for a sufficiently small energy ($H = 10^{-8}$) so that the system is in a weakly nonlinear regime. With the physical system at hand, this energy corresponds to an initial angle deflection of $\approx 0.2^\circ$. The time evolution of $\langle P \rangle$ is shown in Fig. 5(a) where we observe saturation to a constant value for each type of excitation [angular deflection time derivative (black curve) and angular deflection (magenta curve)]. In fact, we also plot, in the same figure, the corresponding linear result (dashed curves), and we observe that the weak nonlinearity does not affect the participation number. Nevertheless, we find that nonlinearity plays a significant role on the evolution of $\langle m_2 \rangle$ and β. This is illustrated in Figs. 5(b) and 5(c) where both these quantities are found to increase for the last two decades ($T \gtrsim 10^3$) of the evolution, clearly indicating energy spreading in the system.

To further explore the spreading, it is worthwhile to also investigate the chaoticity of the system using the finite-time maximum Lyapunov exponent (ftMLE). It is often found, in systems with multiple degrees of freedom, that energy spreading is due to chaos around the excitation region.[4,62,63] The ftMLE,

$$\Lambda(T) = \frac{1}{T} \ln \frac{||\mathbf{w}(T)||}{||\mathbf{w}(0)||}, \tag{16}$$

is computed using the so-called standard method.[64,65] $\mathbf{w}(T)$ is a vector of small perturbations from the phase space trajectory at time T (also called the deviation vector), which we denote as

$$\begin{aligned} \mathbf{w}(T) = [&\delta U_1(T), \ldots, \delta U_N(T), \\ &\delta\theta_1(T), \ldots, \delta\theta_N(T), \\ &M_1 \delta \dot{U}_1(T), \ldots, M_N \delta \dot{U}_N(T), \\ &\Gamma_1 \delta\dot{\theta}_1(T), \ldots, \Gamma_N \delta\dot{\theta}_N(T)], \end{aligned} \tag{17}$$

where $\delta U_n(T)$ and $\delta\theta_n(T)$ indicate small perturbations in positions, while $M_n \delta \dot{U}_n(T)$ and $\Gamma_n \delta\dot{\theta}_n(T)$ indicate small perturbations in momenta for the two DoFs at the nth lattice site. The MLE is defined as $\lambda = \lim_{T\to\infty} \Lambda(T)$. In Eq. (16), $||\cdot||$ denotes the usual Euclidean vector norm. The MLE can be used to discriminate between regular and chaotic motions since $\lambda = 0$ for regular orbits and $\lambda > 0$ for chaotic orbits. The magnitude of the MLE can also be used as a measure of the chaoticity: larger MLE values imply stronger chaotic behaviors. More specifically, for chaotic trajectories, Λ attains a finite positive value, while for regular orbits (for which $\lambda = 0$), Λ decreases to zero following a power law $\Lambda \propto T^{-1}$ (see Sec. 5.3. of

Ref. 65 and references therein). An efficient and accurate method to follow the evolution of $\mathbf{w}(T)$ is to numerically integrate the so-called variational equations,[66] which govern the vector's dynamics, together with the Hamilton equations of motion using the tangent map method outlined in Refs. 67–69.

In Fig. 5(d), we show the calculated ftMLE, which is found to follow the power law decay $\langle \Lambda \rangle \propto T^{-1}$, and thus, the system does not exhibit chaotic behavior, at least up to the times reached in our numerical simulations. We note the presence of even weak, localized chaos, for which P and m_2 do not show signs of an increase, results to the deviation from the law $\Lambda \propto T^{-1}$, making the time evolution of Λ a very sensitive diagnostic tool of chaotic behavior. Thus, we conclude that the observed energy spreading *cannot* be attributed to chaoticity as is the case for other lattice models, including the single DoF per site KG lattice.[62,63,70]

In order to explain the spreading, we need to further monitor the energy density in the lattice as a function of time. In Fig. 6(a), we show four snapshots of the energy density around the initial excitation point ($n = 0$). The spatial distribution of energy is separated into two distinct regions: a large amount of energy localized around $n = 0$ and an extended tail with much lower energy (five orders of magnitude less). In fact, if we consider the propagation of the higher energy central part, especially for $T \lesssim 10^3$, we clearly observe a leading wave-front (dashed vertical lines), which propagates slower than the main leading wave-front. The latter corresponds to the low energy regions [$H_n \lesssim 10^{-13}$ in Fig. 6(a)], which propagates with a normalized velocity close to one. On the contrary, the high energy part around the center [$H_n \gtrsim 10^{-13}$] is propagating much slower with a normalized velocity of ≈ 0.1. These two velocities correspond, respectively, to the largest group velocities of the translation and rotational branches of the dispersion relations shown in Fig. 2. Thus, we conjecture that the two distinct parts of the energy distribution, high and low, correspond, respectively, to the two different types of DoFs, i.e., the rotational and translation deflections.

Furthermore, as shown by the snapshots for $T \gtrsim 10^4$ in Fig. 6(a), at later times, only the lower (translation) part of the energy continues to spread. This fact is corroborated by calculating the exponent of the second moment for energies lower (larger) than a threshold ($H = 10^{-13}$) as shown in Fig. 6(b). The exponent β for the high energy central part almost vanishes (red curve), indicating no spreading, while for the low energy region value of β (black curve) is finite revealing spreading. Thus, we conclude this subsection by explaining the dynamics in the following manner. In the weakly nonlinear regime, the role of the nonlinearity is to induce spreading by stimulating the translation DoFs (which have an FPUT character) through the nonlinear coupling. In this way, the energy spreading in this regime is characterized by a hybrid of KG-like and FPUT-like behaviors. In addition, the rate of wave-packet spreading as quantified by β shows no defined asymptotic behavior but rather a dependency on time [Fig. 5(c)]. This is in accordance with the results obtained for a weakly nonlinear FPUT lattice by Lepri *et al.*[23]

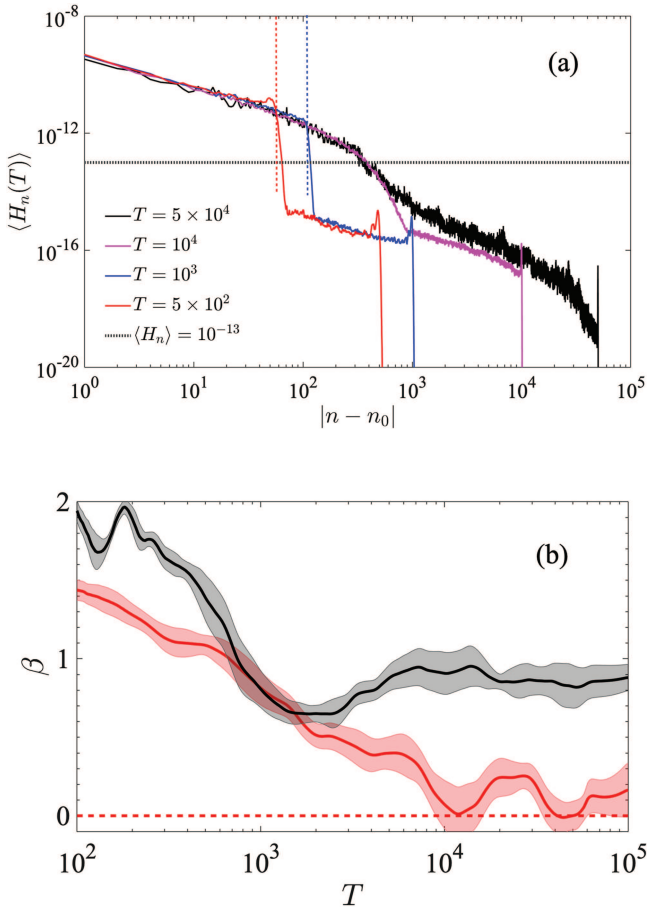

FIG. 6. (a) Average energy distribution profiles of 100 disorder realizations for $T = 5 \times 10^2$ (red curve) , $T = 10^3$ (blue curve), $T = 10^4$ (magenta curve), and $T = 5 \times 10^4$ (black curve). The dotted horizontal line marks the energy $\langle H_n \rangle = 10^{-13}$, while the vertical dashed lines indicate the position of the slower wave-front at the indicated times. (b) Time evolution of the exponents β for the central part (solid red curve) and the tails (solid black curve). The lightly shaded regions in (b) indicate the statistical error (one standard deviation). All panels are for angular deflections of system energy $H = 10^{-8}$.

B. Strongly nonlinear regime

Let us move away from the weakly nonlinear regime and increase the nonlinearity of the system by increasing the initial excitation energy to $H = 5 \times 10^{-3}$. This energy corresponds to large initial angle deflections of about 30°. Note that this value of energy leads to strong nonlinear behavior. The system, in this regime, shows a completely different behavior of spreading as is indicated by the increase of $\langle P \rangle$ during the time evolution as shown in Fig. 7(a). The number of highly excited sites grows in time contrary to what we observed for the weakly nonlinear regime, which shows practically no growth in $\langle P \rangle$ at long times. As expected, this increase of participating particles leads to wave-packet spreading, and this is confirmed by the time evolution of $\langle m_2 \rangle$, which is also increasing as indicated in Fig. 7(b). A feature we observe in this strong nonlinear regime is that the dynamics no longer depends on the type of initial condition (angular deflections or time derivatives of

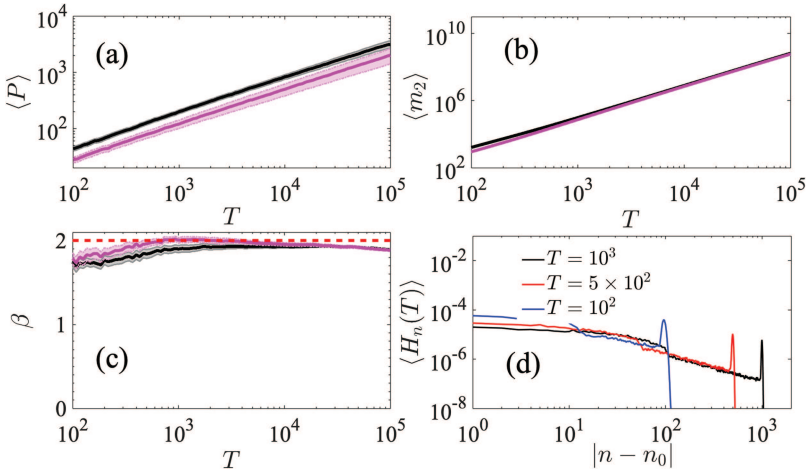

FIG. 7. (a)–(c) Similar to Figs. 5(a)–5(c). (d) Average energy density profiles over 100 disorder realizations at $T = 10^2$ (blue curve), $T = 5 \times 10^2$ (red curve), and $T = 10^3$ (black curve). Results in all panels are for energy $H = 5 \times 10^{-3}$.

angular deflections). This is noticeable from the practically overlapping black (time derivatives of angular deflections) and magenta (angular deflections) curves in Figs. 7(b) and 7(c). To quantify wavepacket spreading, we estimate the exponent of $\langle m_2 \rangle \propto T^{\beta}$, which is found to acquire values around $\beta \approx 2$ as shown in Fig. 7(c). This value indicates very strong spreading corresponding to a near ballistic propagation. We find this result to be quite interesting since the nonlinearity of the flexible architected material under study is strong enough to bring the system to ballistic behavior, which is not always the case in other systems, such as the FPUT and KG lattices.[21,71] In fact, the other example to our knowledge, where near ballistic behavior in a disordered system is observed, is for mechanical lattices featuring non-smooth nonlinearities due to Hertzian forces.[11]

Also, in this strongly nonlinear regime, the distinct behavior of the two types of DoFs that was observed in Fig. 6(a) is now lost. According to Fig. 7(d), by showing the mean profile of the energy distribution, we identify a large part of the energy being localized around the center and a propagating tail traveling almost ballistically. This is expected since according to Eqs. (2) and (3), the coupling of the two types of DoFs is enhanced at each lattice site when the rotations are of high amplitude. Thus, we no longer distinguish between a KG-like and FPUT-like evolution of the energy profiles. We have also considered a range of system energies between $H = 10^{-8}$ and 10^{-3} and found that the distinction between KG- and FPUT-like behaviors gradually disappears as the system energy is increased. Some of the results for the intermediate energies are reported in Ref. 72.

Regarding the chaoticity of the system, for such high initial angles and thus strong nonlinearity, we find the dynamics to be chaotic. This is evident in Fig. 8(a) where the mean value of the ftMLE Λ equation (16) is shown to be decreasing in a much slower rate compared to regular dynamics (dashed line). This type of chaotic behavior, where the ftMLE does not reach an asymptotic constant value, has recently attracted much attention and appears to be a particular case of chaos spreading,[4,31,63] and it is related to the fact that as the wave-packet spreads, the constant total energy is shared among more sites and consequently, the energy per excited site (which plays the role of active nonlinearity strength) decreases. Consequently, the ftMLE, which is a global measure of chaos, is also decreasing.

However, different to what was found in Refs. 4, 31, and 63, for the architected lattice under study, here, the slope of $\langle \Lambda \rangle$ does not reach a constant value even for the *largest possible* angular deflection of 45°. Thus, for the sake of completeness and to be able to compare the results regarding the chaos spreading of the soft architected lattice with other models in the literature, we extend our numerical simulations using even larger initial energies. In particular, in Figs. 8(b) and 8(c), we show results using an initial energy of $H = 10^{-1}$. Note that this value of energy leads to even stronger nonlinear behavior than the penultimate case above. We also observe in

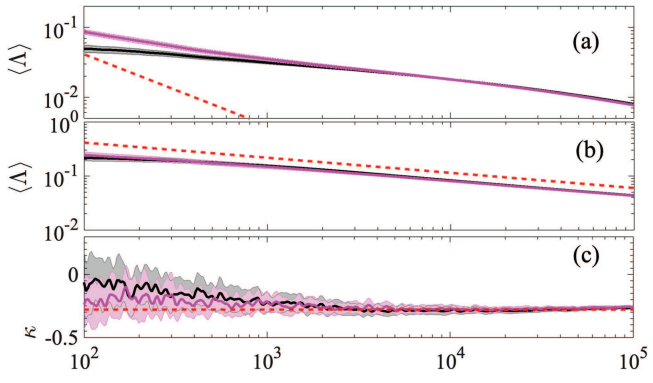

FIG. 8. (a) Time evolution of the average ftMLE, Eq. (16), $\langle \Lambda \rangle$ for the strongly nonlinear regime angular deflections and time derivatives of angular deflections as initial excitations for energy $H = 5 \times 10^{-3}$. The red dashed line indicates the power law $\langle \Lambda \rangle \propto T^{-1}$. (b) Similar to (a) but for energy $H = 10^{-1}$. Here, the red dashed line indicates the power law $\langle \Lambda \rangle \propto T^{\kappa}$, with $\kappa = -0.28$. (c) Time evolution of the exponent κ at energy $H = 10^{-1}$. In all panels, the magenta and black curves, respectively, show results for angular deflections and time derivatives of angular deflections as initial excitations. The magenta horizontal dashed line indicates $\kappa = -0.28$.

Fig. 8(b) that the ftMLE reaches a clearly constant slope with which it is decaying. In particular, the slope of the exponent assuming that $\langle \Lambda \rangle \propto T^{\kappa}$ is found to be approximately $\kappa = -0.28$ for both angular deflections and time derivatives of angular deflections. Note that this asymptotic value of the exponent κ is comparable to the corresponding values for the ftMLE in the more studied cases of 1D lattices, namely, the disordered DNLS equation and the disordered KG model.[62,63] More precisely, the value -0.28 lies between the values obtained for the so-called weak ($\kappa = -0.25$) and strong chaos ($\kappa = -0.3$) regimes of these 1D models having a single DoF per lattice site.

IV. SUMMARY AND CONCLUSIONS

We have studied numerically energy spreading and chaos in a nonlinear disordered architected mechanical lattice. The lattice under consideration describes rotating LEGO® bricks connected with flexible links, which was recently studied experimentally. The in-plane motions of the lattice are described by two DoFs per lattice site, i.e., translations and angular deflections. Furthermore, in the linear limit of the aligned structure, the two DoFs per site are completely decoupled. In this state, the lattice shows two distinct behaviors corresponding to the FPUT and KG-like behaviors for translational and rotational DoFs, respectively. For both cases, we review results regarding the behavior of energy spreading under the effect of disorder.

Using single site angular deflections and time derivatives of angular deflection initial excitations, we studied the system for different strengths of nonlinearity focusing on the weakly nonlinear and strongly nonlinear regimes. For the weakly nonlinear regime, we have shown that the total energy density of the lattice is split into two parts: (i) a slow spreading part around the excitation point following the KG-like behavior and (ii) the fast propagating tails of lower energy, which travel with the speed of sound of the corresponding FPUT lattice and are responsible for the evolution of the second moment of the total energy distribution. For sufficiently large initial excitations, the strong nonlinearity of the flexible architected lattice forces the initial wave-packet to spread ballistically and the distinction between a KG- and an FPUT-like behavior is lost. We note here that a ballistic behavior under strong disorder is not easily achieved, and here, the responsible physical mechanism is the large geometrical nonlinearity.

Additionally, we show that chaos is found to persist during the energy spreading, although its strength decreases in time as quantified by the evolution of the system's ftMLE. Here, the power law time evolution of the exponent of the ftMLE is found to acquire a value that lies between the ones obtained for the so-called weak and strong chaos regimes of the well studied nonlinear KG lattice.

Our results show that flexible architected elastic lattices with coupled DoFs per site provide a modern physical platform to study and observe rich wave dynamics, which cannot otherwise be seen with classical uncoupled fundamental models. Some interesting directions arise from our results, such as the study and manipulation of energy propagation by tuning the dispersion characteristics of rotations, by changing the shear and bending stiffness. Furthermore, here, we only considered an aligned structure where the two DoFs per site are uncoupled in the linear limit. Extensions to other geometries, where the linear modes are polarized, will probably reveal a variety of spreading characteristics and provide a means of controlling energy transport in highly heterogeneous lattices.

ACKNOWLEDGMENTS

A.N. acknowledges funding from the University of Cape Town (University Research Council, URC) postdoctoral fellowship grant and support from the Oppenheimer Memorial Trust (OMT) under Grant No. 21831/01. Ch.S. thanks the Université du Mans for its hospitality during his visits when part of this work was carried out. We thank the Centre for High Performance Computing[73] for providing computational resources for performing significant parts of this paper's computations. We also thank V. Tournat for useful discussions as well as two anonymous referees for their constructive criticism, which helped us improve the content and the presentation of our work.

AUTHOR DECLARATIONS

Conflict of Interest

The authors have no conflicts to disclose.

DATA AVAILABILITY

The data that support the findings of this study are available within the article.

REFERENCES

[1] F. J. Dyson, "The dynamics of a disordered linear chain," Phys. Rev. **92**, 1331 (1953).
[2] J. D. Bodyfelt, T. Laptyeva, G. Gligoric, D. Krimer, C. Skokos, and S. Flach, "Wave interactions in localizing media—A coin with many faces," Int. J. Bifurcation Chaos **21**, 2107–2124 (2011).
[3] F. M. Izrailev, A. A. Krokhin, and N. Makarov, "Anomalous localization in low-dimensional systems with correlated disorder," Phys. Rep. **512**, 125–254 (2012).
[4] M. Ivanchenko, T. Laptyeva, and S. Flach, "Quantum chaotic subdiffusion in random potentials," Phys. Rev. B **89**, 060301 (2014).
[5] P. W. Anderson, "Absence of diffusion in certain random lattices," Phys. Rev. **109**, 1492 (1958).
[6] R. Bruinsma and S. Coppersmith, "Anderson localization and breakdown of hydrodynamics in random ferromagnets," Phys. Rev. B **33**, 6541 (1986).
[7] T. Schwartz, G. Bartal, S. Fishman, and M. Segev, "Transport and Anderson localization in disordered two-dimensional photonic lattices," Nature **446**, 52–55 (2007).
[8] Y. Lahini, A. Avidan, F. Pozzi, M. Sorel, R. Morandotti, D. N. Christodoulides, and Y. Silberberg, "Anderson localization and nonlinearity in one-dimensional disordered photonic lattices," Phys. Rev. Lett. **100**, 013906 (2008).
[9] J. Billy, V. Josse, Z. Zuo, A. Bernard, B. Hambrecht, P. Lugan, D. Clément, L. Sanchez-Palencia, P. Bouyer, and A. Aspect, "Direct observation of Anderson localization of matter waves in a controlled disorder," Nature **453**, 891–894 (2008).
[10] G. Roati, C. D'Errico, L. Fallani, M. Fattori, C. Fort, M. Zaccanti, G. Modugno, M. Modugno, and M. Inguscio, "Anderson localization of a non-interacting Bose–Einstein condensate," Nature **453**, 895–898 (2008).
[11] E. Kim, A. J. Martínez, S. E. Phenisee, P. Kevrekidis, M. A. Porter, and J. Yang, "Direct measurement of superdiffusive energy transport in disordered granular chains," Nat. Commun. **9**, 1 (2018).
[12] W. A. Harrison, *Electronic Structure and the Properties of Solids: The Physics of the Chemical Bond* (Courier Corporation, 2012).
[13] C. Rogers and T. B. Moodie, *Wave Phenomena: Modern Theory and Applications* (Elsevier, 1984).

[14]H. Matsuda and K. Ishii, "Localization of normal modes and energy transport in the disordered harmonic chain," Prog. Theor. Phys. Suppl. **45**, 56–86 (1970).
[15]K. Ishii, "Localization of eigenstates and transport phenomena in the one-dimensional disordered system," Prog. Theor. Phys. Suppl. **53**, 77–138 (1973).
[16]P. Datta and K. Kundu, "Energy transport in one-dimensional harmonic chains," Phys. Rev. B **51**, 6287 (1995).
[17]G. Gallavotti, *The Fermi-Pasta-Ulam Problem: A Status Report* (Springer, 2007), Vol. 728.
[18]P. G. Kevrekidis, *The Discrete Nonlinear Schrödinger Equation: Mathematical Analysis, Numerical Computations and Physical Perspectives* (Springer Science & Business Media, 2009), Vol. 232.
[19]G. Theocharis, N. Boechler, and C. Daraio, "Nonlinear periodic phononic structures and granular crystals," in *Acoustic Metamaterials and Phononic Crystals* (Springer, 2013), pp. 217–251.
[20]P. A. Deymier, "Introduction to phononic crystals and acoustic metamaterials," in *Acoustic Metamaterials and Phononic Crystals* (Springer, 2013), pp. 1–12.
[21]S. Flach, "Nonlinear lattice waves in random potentials," in *Nonlinear Optical and Atomic Systems* (Springer, 2015), pp. 1–48.
[22]S. Gredeskul and L. Pastur, "One-dimensional localization and wave propagation in linear and nonlinear media," in *Nonlinearity with Disorder* (Springer, 1992), pp. 126–133.
[23]S. Lepri, R. Schilling, and S. Aubry, "Asymptotic energy profile of a wave packet in disordered chains," Phys. Rev. E **82**, 056602 (2010).
[24]L. Ponson, N. Boechler, Y. M. Lai, M. A. Porter, P. Kevrekidis, and C. Daraio, "Nonlinear waves in disordered diatomic granular chains," Phys. Rev. E **82**, 021301 (2010).
[25]M. Manjunath, A. P. Awasthi, and P. H. Geubelle, "Wave propagation in random granular chains," Phys. Rev. E **85**, 031308 (2012).
[26]A. J. Martínez, P. G. Kevrekidis, and M. A. Porter, "Superdiffusive transport and energy localization in disordered granular crystals," Phys. Rev. E **93**, 022902 (2016).
[27]V. Achilleos, G. Theocharis, and C. Skokos, "3Energy transport in one-dimensional disordered granular solids," Phys. Rev. E **93**, 022903 (2016).
[28]R. K. Shrivastava and S. Luding, "Effect of disorder on bulk sound wave speed: A multiscale spectral analysis," Nonlinear Process. Geophys. **24**, 435–454 (2017).
[29]M. Przedborski, S. Sen, and T. A. Harroun, "The equilibrium phase in heterogeneous Hertzian chains," J. Stat. Mech.: Theory Exp. **2017**, 123204.
[30]A. Ngapasare, G. Theocharis, O. Richoux, C. Skokos, and V. Achilleos, "Chaos and Anderson localization in disordered classical chains: Hertzian versus Fermi-Pasta-Ulam-Tsingou models," Phys. Rev. E **99**, 032211 (2019).
[31]B. M. Manda, B. Senyange, and C. Skokos, "Chaotic wave-packet spreading in two-dimensional disordered nonlinear lattices," Phys. Rev. E **101**, 032206 (2020).
[32]M. I. N. Rosa and M. Ruzzene, "Dynamics of 'small-world' network phononic lattices: Spectral gaps and diffusive transport," arXiv:2203.10381 (2022).
[33]H.-Y. Xie, V. E. Kravtsov, and M. Müller, "Anderson localization of one-dimensional hybrid particles," Phys. Rev. B **86**, 014205 (2012).
[34]X. Yu and S. Flach, "Enhancement of chaotic subdiffusion in disordered ladders with synthetic gauge fields," Phys. Rev. E **90**, 032910 (2014).
[35]A. Ngapasare, G. Theocharis, O. Richoux, C. Skokos, and V. Achilleos, "Wave propagation in a strongly disordered one-dimensional phononic lattice supporting rotational waves," Phys. Rev. B **102**, 054201 (2020).
[36]H. Pichard, A. Duclos, J.-P. Groby, V. Tournat, and V. Gusev, "Localized transversal-rotational modes in linear chains of equal masses," Phys. Rev. E **89**, 013201 (2014).
[37]F. Allein, V. Tournat, V. Gusev, and G. Theocharis, "Transversal–rotational and zero group velocity modes in tunable magneto-granular phononic crystals," Extreme Mech. Lett. **12**, 65–70 (2017).
[38]H. Yasuda, T. Tachi, M. Lee, and J. Yang, "Origami-based tunable truss structures for non-volatile mechanical memory operation," Nat. Commun. **8**, 962 (2017).
[39]H. Yasuda and J. Yang, "Tunable frequency band structure of origami-based mechanical metamaterials," J. Int. Assoc. Shell Spat. Struct. **58**, 287–294 (2017).
[40]B. Deng, P. Wang, Q. He, V. Tournat, and K. Bertoldi, "Metamaterials with amplitude gaps for elastic solitons," Nat. Commun. **9**, 1 (2018).
[41]F. Allein, V. Tournat, V. Gusev, and G. Theocharis, "Linear and nonlinear elastic waves in magnetogranular chains," Phys. Rev. Appl. **13**, 024023 (2020).
[42]R. F. Shepherd, F. Ilievski, W. Choi, S. A. Morin, A. A. Stokes, A. D. Mazzeo, X. Chen, M. Wang, and G. M. Whitesides, "Multigait soft robot," Proc. Natl. Acad. Sci. U.S.A. **108**, 20400–20403 (2011).
[43]D. Yang, B. Mosadegh, A. Ainla, B. Lee, F. Khashai, Z. Suo, K. Bertoldi, and G. M. Whitesides, "Buckling of elastomeric beams enables actuation of soft machines," Adv. Mater. **27**, 6323–6327 (2015).
[44]D. J. Beebe, J. S. Moore, J. M. Bauer, Q. Yu, R. H. Liu, C. Devadoss, and B.-H. Jo, "Functional hydrogel structures for autonomous flow control inside microfluidic channels," Nature **404**, 588–590 (2000).
[45]S. Shan, S. H. Kang, J. R. Raney, P. Wang, L. Fang, F. Candido, J. A. Lewis, and K. Bertoldi, "Multistable architected materials for trapping elastic strain energy," Adv. Mater. **27**, 4296–4301 (2015).
[46]D. Restrepo, N. D. Mankame, and P. D. Zavattieri, "Phase transforming cellular materials," Extreme Mech. Lett. **4**, 52–60 (2015).
[47]B. Florijn, C. Coulais, and M. van Hecke, "Programmable mechanical metamaterials," Phys. Rev. Lett. **113**, 175503 (2014).
[48]K. Nakajima, H. Hauser, T. Li, and R. Pfeifer, "Information processing via physical soft body," Sci. Rep. **5**, 10487 (2015).
[49]K. Bertoldi and M. Boyce, "Mechanically triggered transformations of phononic band gaps in periodic elastomeric structures," Phys. Rev. B **77**, 052105 (2008).
[50]S. Rudykh and M. C. Boyce, "Transforming wave propagation in layered media via instability-induced interfacial wrinkling," Phys. Rev. Lett. **112**, 034301 (2014).
[51]P. Wang, F. Casadei, S. Shan, J. C. Weaver, and K. Bertoldi, "Harnessing buckling to design tunable locally resonant acoustic metamaterials," Phys. Rev. Lett. **113**, 014301 (2014).
[52]P. Celli and S. Gonella, "Manipulating waves with LEGO® bricks: A versatile experimental platform for metamaterial architectures," Appl. Phys. Lett. **107**, 081901 (2015).
[53]Each cross unit in Fig. 1(a) has horizontal and vertical components of mass $m^{\dagger} = m_n^{\dagger} = 2.4537$ g (homogeneous case) whose length and width are, respectively, $d = 38$ mm and $b = 6$ mm. Following Ref. 40, the moment of inertia of the overlapping part is considered to be negligible. As an example, disorder in the system can be introduced by taking crosses of different material density for each n*th* site but keeping the geometry unaltered. The resultant effect of such an action would introduce disorder in $m_n^{\dagger}$, which implies also disorder in J_n.
[54]S. Blanes, F. Casas, A. Farres, J. Laskar, J. Makazaga, and A. Murua, "New families of symplectic splitting methods for numerical integration in dynamical astronomy," Appl. Numer. Math. **68**, 58–72 (2013).
[55]B. Senyange and C. Skokos, "Computational efficiency of symplectic integration schemes: Application to multidimensional disordered Klein–Gordon lattices," Eur. Phys. J. Spec. Top. **227**, 625–643 (2018).
[56]C. Danieli, B. M. Manda, T. Mithun, and C. Skokos, "Computational efficiency of numerical integration methods for the tangent dynamics of many-body hamiltonian systems in one and two spatial dimensions," Math. Eng. **1**, 447–488 (2019).
[57]W. S. Cleveland, "LOWESS: A program for smoothing scatterplots by robust locally weighted regression," Am. Stat. **35**, 54 (1981).
[58]W. S. Cleveland and S. J. Devlin, "Locally weighted regression: An approach to regression analysis by local fitting," J. Am. Stat. Assoc. **83**, 596–610 (1988).
[59]Y. S. Kivshar and M. Peyrard, "Modulational instabilities in discrete lattices," Phys. Rev. A **46**, 3198 (1992).
[60]Y. S. Kivshar, "Creation of nonlinear localized modes in discrete lattices," Phys. Rev. E **48**, 4132 (1993).
[61]M. Johansson, "Discrete nonlinear Schrödinger approximation of a mixed Klein–Gordon/Fermi–Pasta–Ulam chain: Modulational instability and a statistical condition for creation of thermodynamic breathers," Physica D **216**, 62–70 (2006).
[62]C. Skokos, I. Gkolias, and S. Flach, "Nonequilibrium chaos of disordered nonlinear waves," Phys. Rev. Lett. **111**, 064101 (2013).
[63]B. Senyange, B. M. Manda, and C. Skokos, "Characteristics of chaos evolution in one-dimensional disordered nonlinear lattices," Phys. Rev. E **98**, 052229 (2018).
[64]G. Benettin, L. Galgani, A. Giorgilli, and J.-M. Strelcyn, "Lyapunov characteristic exponents for smooth dynamical systems and for Hamiltonian systems; A method for computing all of them. Part 1: Theory," Meccanica **15**, 9–20 (1980).

[65]C. Skokos, "The Lyapunov characteristic exponents and their computation," in *Dynamics of Small Solar System Bodies and Exoplanets* (Springer, 2010), pp. 63–135.
[66]G. Contopoulos, L. Galgani, and A. Giorgilli, "On the number of isolating integrals in Hamiltonian systems," Phys. Rev. A **18**, 1183 (1978).
[67]C. Skokos and E. Gerlach, "Numerical integration of variational equations," Phys. Rev. E **82**, 036704 (2010).
[68]E. Gerlach and C. Skokos, "Comparing the efficiency of numerical techniques for the integration of variational equations," AIMS Proc. **2011**, 475–484 (2011).
[69]E. Gerlach, S. Eggl, and C. Skokos, "Efficient integration of the variational equations of multidimensional Hamiltonian systems: Application to the Fermi–Pasta–Ulam lattice," Int. J. Bifurcation Chaos **22**, 1250216 (2012).
[70]B. Senyange and C. Skokos, "Identifying localized and spreading chaos in nonlinear disordered lattices by the Generalized Alignment Index (GALI) method," Physica D **432**, 133154 (2022).
[71]M. Mulansky and A. Pikovsky, "Energy spreading in strongly nonlinear disordered lattices," New J. Phys. **15**, 053015 (2013).
[72]A. Ngapasare, "Waves in disordered and nonlinear mechanical structures," Ph.D. thesis (Le Mans, 2020).
[73]https://www.chpc.ac.za.